Deformation microstructures of low- and high-strain epidote-blueschist (Ryukyu arc, Japan): Implications for subduction interface rheology

Sara De Caroli [a,*], Åke Fagereng [a], Kohtaro Ujiie [b], Thomas Blenkinsop [a], Francesca Meneghini [c], Duncan Muir [a]

[a] School of Earth and Environmental Sciences, Cardiff University, CF10 3AT, Cardiff, United Kingdom
[b] Graduate School of Science and Technology Sciences, University of Tsukuba, 1-1-1 Tennodai, Tsukuba, 305-8572, Japan
[c] Dipartimento di Scienze della Terra, Università degli Studi di Pisa, 56126, Pisa, Italy

ARTICLE INFO

ABSTRACT

We present field and microstructural data from an exhumed subduction complex in the Ryukyu arc, Japan, where epidote-blueschist, Triassic, Tomuru metamorphic rocks with block-in-matrix structure crop out. With the aim to constrain epidote-blueschist rheology, we investigate fabric development and infer deformation mechanisms of blocks and matrix through microstructural analyses on the main fabric-forming minerals: glaucophane, epidote and albite. The blocks have a poorly developed, discontinuous foliation. In contrast, the matrix has a well-developed, continuous foliation. Glaucophane is the principal foliation-forming phase, arranged in inter-connected layers that surround epidote and albite, which suggests that glaucophane controls epidote-blueschist rheology. Deformation mechanisms inferred from petrographic and electron backscatter diffraction (EBSD) analysis are similar in blocks and matrix, with glaucophane deformed by diffusion creep accompanied by reaction-driven creep, albite by diffusion creep, and epidote by brittle fracture and incipient dislocation creep, based on degrees of internal misorientations, lattice preferred orientation (LPO) development and grain size. During deformation, shear stress must have been relatively low, which is implied by the predominance of diffusion and reaction creep as the dominant deformation mechanisms, and by the small viscosity contrast between blocks and matrix, reflected by their similarity in dominant deformation mechanism.

1. Introduction

In convergent margins, the subducting and overriding plates are separated by a kilometres-thick plate boundary shear zone, also referred to as subduction megathrust. The subduction megathrust is typically thought of as a heterogeneously strained mélange of rocks, which have heterogeneous composition and a wide range of rheological properties that evolve with progressive deformation and metamorphism (Fisher and Byrne, 1987; Fagereng and Sibson, 2010; Rowe et al., 2013; Oncken et al., 2022). Subduction megathrust segments accommodate a variety of geophysically-observed fault slip styles varying from steady creep through a range of transient, slow earthquake phenomena to fast, episodic earthquake slip (Peng and Gomberg, 2010). The downdip limit for earthquake nucleation is controlled by the depth where rock behaviour changes from frictional to viscous. This transition tends to occur at 350–450 °C or near the Moho, whichever is shallower (Hyndman et al., 1997). A spectrum of slow earthquakes generally occur

downdip of the seismogenic zone (Peng and Gomberg, 2010; Schwartz and Rokosky, 2007; Obara and Kato, 2016; Behr and Bürgmann, 2021). This region is therefore host to multiple slip speeds, although the participating geological structures and accommodating mineral-scale deformation mechanisms are not well known (Kirkpatrick et al., 2021).

Viscous deformation in the crust occurs predominantly by diffusion creep and dislocation creep. Diffusion creep is the predominant deformation mechanism that prevails at low stress and small grain size in shear zones and implies a linear dependence of strain rate on stress (Tsenn and Carter, 1987). In contrast, power-law creep, where rock behaviour is controlled by dislocation glide and climb, is an intra-granular process independent of grain size, and with a non-linear relationship between strain rate and stress (Weertman, 1968).

At fixed stress and strain rate, small grain sizes promote diffusive mechanisms, whereas larger grain sizes promote dislocation glide and/or climb. Moreover, grain size evolution, for example through grain growth or grain size reduction by metamorphism and/or metasomatism,

---

relates to changes in flow strength and can move the energetically favourable mechanism between diffusion- and dislocation-controlled deformation (Rutter and Brodie, 1988; Montési and Hirth, 2003; Kilian et al., 2011, Lee et al., 2022, Ujjie et al., 2022). In addition, during deformation, syn-tectonic reactions can lead to oriented growth of crystals with changing composition, reflecting syn-kinematic changes in pressure and temperature through zoning (Wintsch and Yi, 2002; Wintsch and Yeh, 2013). Observations on natural and laboratory-deformed samples show that the new mineral phases form in orientations favourable to accommodate shear stress, with a preferred orientation parallel to foliation (Shea and Kroonenberg, 1993). There-fore, there can be a strong control of mineral reactions on the devel-opment of rock fabric, which in turn will lead to weakening (e.g., reaction creep; Wintsch et al., 1995, 2013).

Mafic oceanic rocks and seafloor sediments are the main lithologies involved in deformation along the subduction interface. In particular, blueschist rocks represent the remnants of oceanic crust that have been subducted to high pressure (P) -low temperature (T) metamorphic conditions (Miyashiro, 1961; Ernst, 1973) and are characterised by distinctive mineral assemblages with a foliation typically defined by glaucophane. The P-T range of blueschist stability (e.g., Peacock, 1992) coincides with metamorphic conditions at the depth-range typical of temporally coincident, episodic tremor and slow slip (ETS) in the tran-sition zone downdip of the seismogenic zone (typically, but not exclu-sively, 30–50 km and in excess of 300 °C) (Rogers and Dragert, 2003; Obara et al., 2004; Obara and Kato, 2016). In this depth and temperature range, tectonic displacement is accommodated by geodetically and seismically detected ETS in some places, including segments of the well-instrumented Nankai and Cascadia margins (Obara, 2002; Rogers and Dragert, 2003; Peng and Gomberg, 2010). However, at similar inferred P-T conditions, some subduction zones (e.g., Central Cascadia, Schmalzle et al., 2014) show a combination of ETS and steady fault creep. At the Ryukyu Arc, short-term slow slip events occur with mobile source areas of low frequency earthquakes, which are temporally but not always spatially coincident with the slow slip (Nakamura, 2017; Sue-naga et al., 2021). This variable behaviour is thought to reflect different rheology of the materials on the subduction interface, and consequently different deformation mechanisms active in the rocks deforming at that depth and temperature (Fagereng et al., 2014; Kotowski and Behr, 2019; Behr and Bürgmann, 2021; Kirkpatrick et al., 2021).

Glaucophane and sodic amphiboles (e.g., Leake and Woolley, 1997) define blueschist fabric and are therefore an important control on sub-duction interface rheology downdip of the seismogenic zone. The mechanisms that govern their deformation are critical for understanding megathrust stress state and slip style; however, there is limited literature that analyses the deformation mechanisms prevalent in glaucophane. Previous studies on blue amphiboles relevant to the subduction thrust interface suggest dislocation creep as the dominant deformation mech-anism in glaucophane deformation, on the basis of microstructural and intracrystalline misorientation data (Behr et al., 2018; Kim et al., 2013; Kotowski and Behr, 2019). However, Misch (1969) described micro-structures indicative of synkinematic diffusion creep in Na-amphiboles, and recently Muñoz-Montecinos et al. (2023) described the role of dissolution-precipitation creep in accommodating Na-amphibole defor-mation in the region of subduction interface ETS.

In a broader range of P-T stability and tectonic environments, thus not limited to the HP-LT environments where glaucophane is stable, amphibole group minerals have been interpreted to deform by a variety of deformation mechanisms in both naturally- and laboratory-deformed samples. Some authors suggest dominant dislocation creep represented by intracrystalline features such as subgrains and undulose extinction formed via glide and climb on (100)[001] at high temperatures (Brodie and Rutter, 1985; Reynard and Gillet, 1989) or dislocation glide on (100)[001] (Skrotzki, 1990). In contrast, others highlight the impor-tance of diffusion creep in the formation of amphibole fabric (Getsinger and Hirth, 2014) and, when a reactant aqueous phase is present,

dissolution-precipitation creep (Berger and Stünitz, 1996; Condit and Mahan, 2018; Giuntoli et al., 2018; Muñoz-Montecinos et al., 2023; Lee et al., 2022; Tulley et al., 2020). Additionally, structures resulting from cataclastic flow have been observed in naturally deformed amphibolites at greenschist and amphibolite metamorphic conditions (Imon et al., 2004; Nyman et al., 1992) and at blueschist conditions (Muñoz-Montecinos et al., 2023).

We present data from an exhumed epidote-blueschist subduction complex of Triassic age on Ishigaki Island in the Ryukyu arc, Japan, which we interpret to represent a fossilized subduction shear zone that records deformation downdip of the seismogenic zone. We analyse and compare the deformation characteristics of higher- and lower-strain block-in-matrix epidote-blueschist rocks to understand rheology of subduction interfaces below the seismogenic zone, including the range of depth and temperature where ETS typically occur. First, we address the foliation development, through grain size analyses and mineral shape analyses of foliation-forming glaucophane, epidote and albite. Secondly, we determine which deformation mechanisms were active and whether they varied between blocks and matrix of similar compo-sition but different fabrics.

2. Geologic setting

The island of Ishigaki is part of the Yaeyama islands, set in the southwestern sector of the Ryukyu arc, east of Taiwan. Here the oceanic crust of the Philippine Sea plate subducts towards the NW at 12.5 cm/yr (Heki and Kataoka, 2008) under the Amurian plate along the Ryukyu trench (Lallemand et al., 1999) (Fig. 1A). Oblique convergence of 40° causes important right-lateral strike-slip faults in the upper plate (Lal-lemand et al., 1999). The stratigraphy of Ishigaki island comprises a metamorphic basement, consisting of Triassic Tomuru metamorphic rocks, the Jurassic Fusaki Formation and Eocene Miyara and Nosoko Formations, unconformably overlain by quaternary sediments (Kizaki, 1986; Nuong et al., 2008; Osozawa and Wakabayashi, 2012) (Fig. 1B). The Tomuru metamorphic rocks, the subject of this study, crop out in km-scale anticlinal domes overlain by the sedimentary cover in the northern, central, and western areas of Ishigaki (Osozawa and Waka-bayashi, 2012), and they consist of HP-LT mafic, pelitic and psammitic schists, the latter containing blocks of metamorphosed gabbros and serpentinites, interpreted as originating from the oceanic crust (Nuong et al., 2008). Two types of veins intersect these rocks, and can be clas-sified by composition as quartz-rich and epidote-rich. Quartz-rich veins are abundant in the pelitic schists and at the contact between the mafic and pelitic lithologies and are parallel to subparallel to the main folia-tion. Quartz-rich veins are also present in the mafic schists, but are less abundant than in the pelitic schists. The epidote-rich veins are limited to the mafic schists, occur relatively scattered throughout the studied outcrops, and appear both parallel to and crosscutting the main foliation.

The mafic schists have been divided into three groups based on their mineral assemblages, indicative of different metamorphic grades (Nuong et al., 2008). The lowest grade rocks contain glaucophane, pumpellyite, lawsonite and aragonite, while in the intermediate grade metabasites the pumpellyite, aragonite, lawsonite assemblage is replaced by glaucophane and epidote. In the north of Ishigaki island the highest-grade rocks crop out, containing barroisite in the mafic schists and garnet in the pelitic schists. The boundaries between the three groups of rocks are covered by later sedimentary rocks and cannot be directly observed. K–Ar phengite dating gives metamorphic ages ranging from 208 to 220 Ma for the highest grade metabasites to 188–205 Ma for the lowest grade metabasites. Based on the presence of aragonite, metamorphic conditions have been estimated at $\geq 400\,°C$ and 8–9 kbar (Ishizuka and Imaizumi, 1988).

The paragenesis of the blueschist rocks in this study is characterised by glaucophane, Fe-epidote and albite as the main foliation-forming minerals, along with minor quartz and titanite, and by the absence of
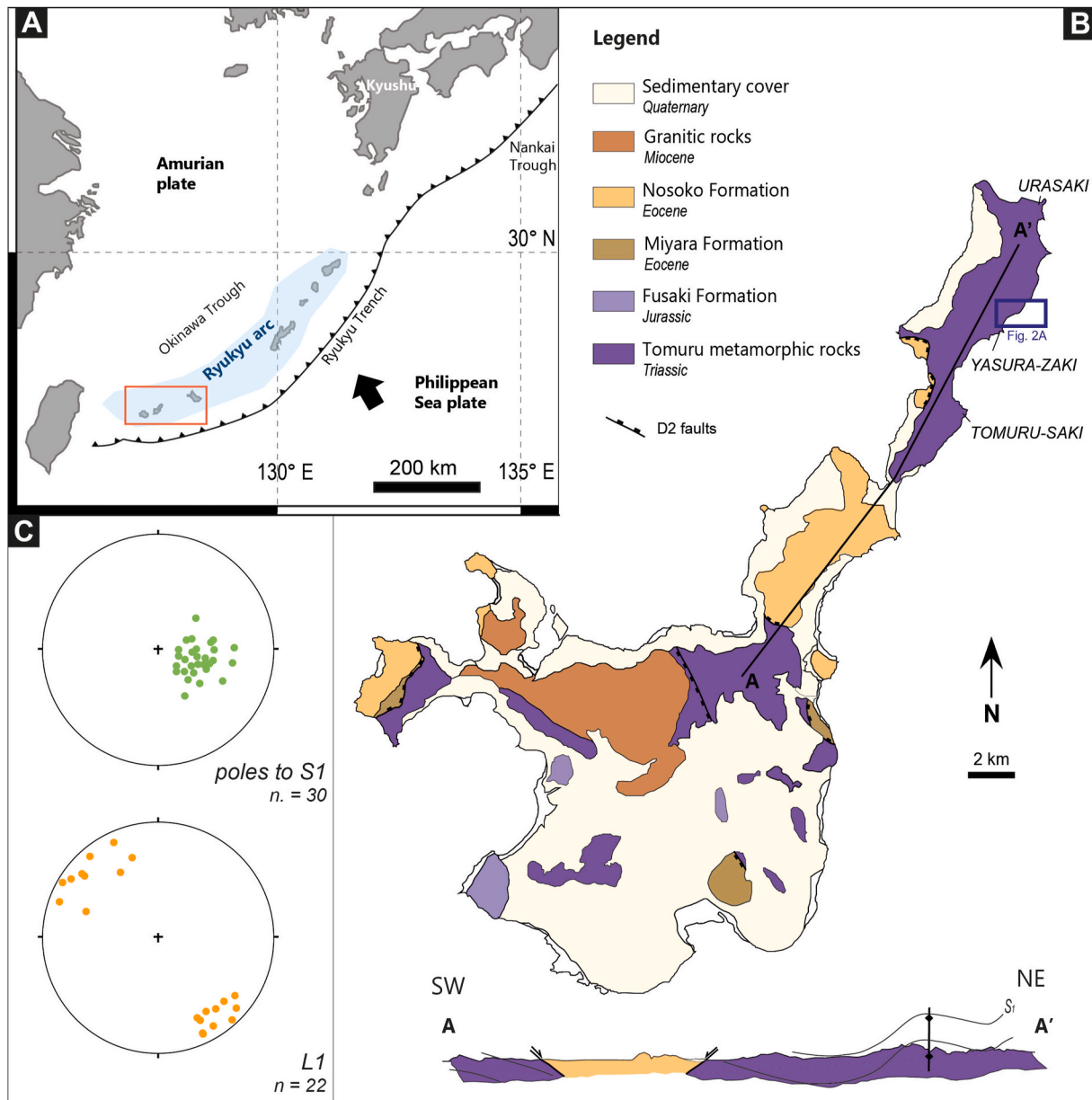
Fig. 1. a) Tectonic setting of the Ryukyu arc, SW Japan. The Philippine Sea Plate subducts towards NW under the Amurian plate along the Ryukyu Trench. Contoured in red, the location of the Yaeyama Islands, where Ishigaki Island is located, in the southernmost sector of the Ryukyu arc; b) geologic map of Ishigaki Island and geologic profile (modified from Osozawa and Wakabayashi, 2012). Contoured in blue, the location of the analysed block-in-matrix epidote-blueschists; c) stereographic equal area projections of the main structures measured in the Tomuru epidote-blueschists, foliation S1 and mineral lineation L1 (n = number of measurements). S1 is generally NNE-SSW striking, with gentle to moderate dips to NW; L1 is dips gently towards SE and NW. (For interpretation of the references to colour in this figure legend, the reader is referred to the Web version of this article.)

lawsonite. This signifies metamorphic conditions at the epidote-blueschist facies, although we cannot exclude that some of the epidote was originally lawsonite during the progressive deformation recorded in the rocks. It is important to consider that epidote and lawsonite do not respond identically to deformation (Kim et al., 2013); however, the approach used in this study should have general applicability to understanding epidote-blueschist rheology, due to the preponderance of foliation-forming glaucophane in most blueschist rocks and given that it is generally abundant in our samples.

Two deformation stages are recognized. The first, D1, resulted in the main foliation S1 striking NNE-SSW with gentle to moderate dips to the NW (Fig. 1C), and it is characterized by stretching lineations (L1, Fig. 1C) and shear structures with a general NW-SE trend and top-to-SE sense of shear (Osozawa and Wakabayashi, 2012). Peak HP-LT

metamorphism is related to the D1 deformation stage based on the mineral paragenesis defining the main foliation S1, characterised by the presence of glaucophane, Fe-epidote and albite with minor quartz and titanite. A second deformation stage, D2, is recognized as folding the S1 schistosity with asymmetric open folds with NE vergence and axial planes dipping gently towards SW (Fig. 1B). The D2 transport direction is subparallel to NE-SW striking strike-slip faults, leading previous authors to hypothesise that the exhumation might have been associated with a significant strike-slip component (Osozawa and Wakabayashi, 2012). The D2 stage is suggested to have accommodated exhumation, including the extrusion of the Tomuru rocks in the core of km-scale anticlinal domes, according to Osozawa and Wakabayashi (2012). Our microstructural observations are limited to the epidote-blueschist mafic schists of the Tomuru metamorphic rocks, sampled where D1 structures

and S1 foliation dominate and the rocks are not markedly affected by D2 deformation.

3. Field observations

The mafic schists of the Tomuru metamorphic rocks crop out in a block-in-matrix structure characterised by epidote-blueschist facies mineral assemblages, with a fine-grained matrix embedding multi-dm sized blocks, including both epidote-blueschist and greenschist mineral assemblages (Fig. 2A). Throughout the rock volume, greenschist blocks and epidote-blueschist blocks are present in similar abundance.

The matrix contains a uniform fabric, characterised by a NE-SW striking sub-mm-spaced foliation that wraps around the blocks, and a well-developed NW-SE trending mineral lineation defined by the preferred alignment of glaucophane and albite, which is interpreted as a stretching lineation (Fig. 2B). The blocks, both greenschist and epidote-blueschist, generally have poorly foliated cores and well-foliated rims. At the outcrop scale, the only difference between epidote-blueschist blocks and matrix is the foliation development; there is no discernible difference in colour or mineralogy, and any grain size difference is minor. The cores show a mm-spaced internal foliation (Fig. 2D), which is aligned with the general NE-SW strike of the matrix, and a similar but less developed NW-SE trending mineral lineation as that seen in the matrix, whereas the rims present a fabric that is similar to that of the epidote-blueschist matrix, with a sub-mm spaced foliation, NE-SW

striking (Fig. 2C,E).

4. Methods

A total of 11 samples of epidote-blueschist rocks were used for microstructural observations, and two representative samples were chosen for detailed microstructural analyses, each representing block and matrix of the epidote-blueschist Tomuru metamorphic rocks. Hand-samples were cut along the kinematic XZ section of the finite strain ellipsoid, where the X-axis is parallel to the stretching lineation, defined in both samples by the preferred alignment of glaucophane and albite grains, and the Z-axis is perpendicular to foliation. Foliation-forming glaucophane, epidote and albite were analysed on polished carbon-coated thin sections using the Zeiss Sigma HD Field Emission Gun scanning electron microscope (SEM) in the School of Earth and Environmental Sciences at Cardiff University equipped with two Oxford Instruments energy-dispersive spectroscopy detectors (EDS).

Electron backscatter diffraction (EBSD) patterns were acquired with a Nordlys Oxford Instruments detector and 20 kV accelerating voltage, 14–22 mm working distance and 0.5–2 μm step size on a 70° tilted sample. EBSD data were analysed using automated procedures in the MTEX toolbox (Bachmann et al., 2010) in MATLAB to obtain grain maps of block and matrix, mineral proportions, to carry out fabric analyses and to provide crystallographic orientation data for the principal foliation-forming components of the rocks: glaucophane, epidote and
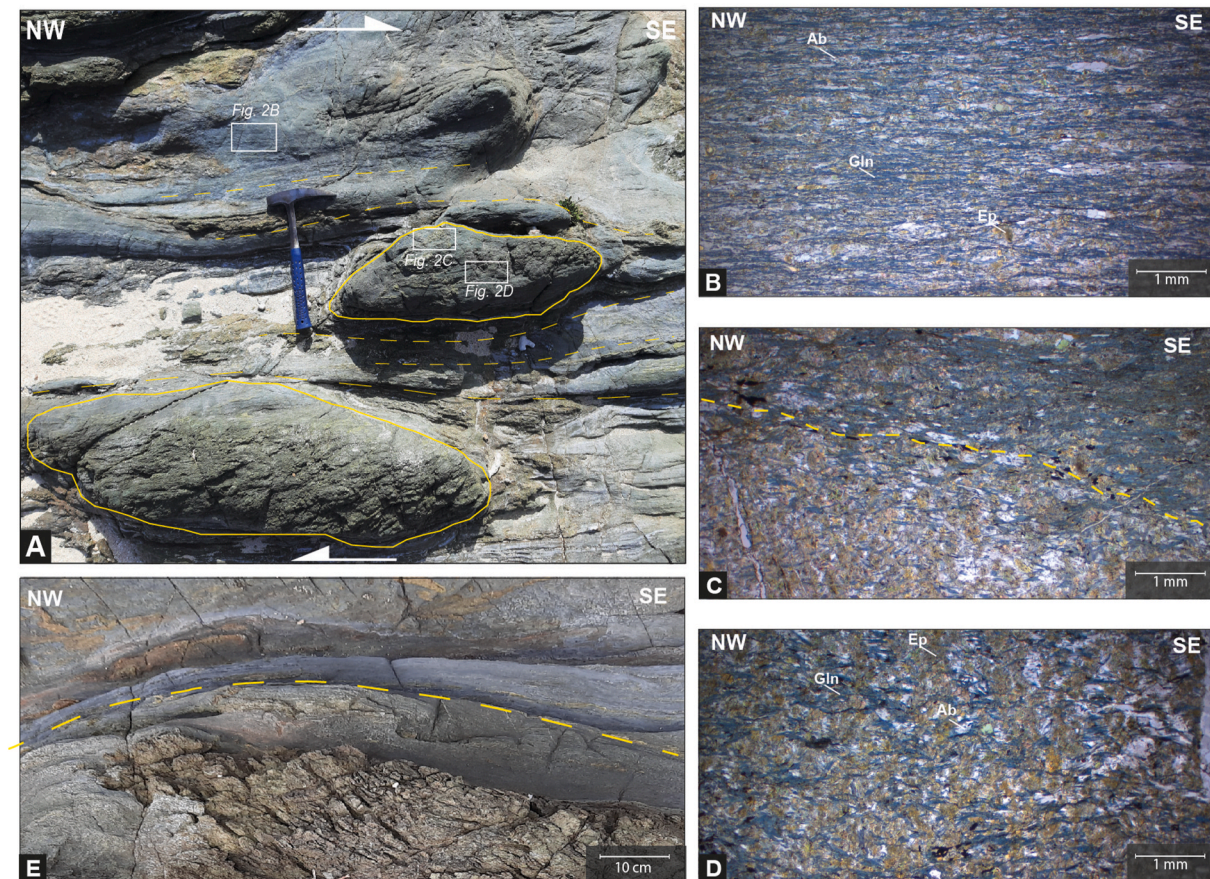

Fig. 2. a) Mesoscale block-in-matrix structure of the Tomuru metamorphic rocks. Contoured in yellow, the epidote-blueschist blocks are embedded in a well-foliated epidote-blueschist matrix; b) photomicrograph of the well-foliated epidote-blueschist matrix analysed in this paper, where continuous layers of glaucophane alternate with domains of epidote, albite and minor quartz and titanite; c) photomicrograph of the epidote-blueschist block rim. The yellow dashed-line separates the poorly foliated fabric of the block core (bottom left of image) from the well-foliated fabric of the core rim (top right of image); d) photomicrograph of the poorly foliated epidote-blueschist block analysed in this paper. Glaucophane grains are not well interconnected and lie between epidote and albite grains. e) detail of the block margin (bottom left of image) in contact with the epidote-blueschist matrix (top right of image). Note how the block has a poorly foliated core and a well-foliated rim. *Gln: glaucophane, Ep: epidote, Ab: albite.* (For interpretation of the references to colour in this figure legend, the reader is referred to the Web version of this article.)

albite.

4.1. Grain reconstruction and fabric analyses

Grain boundaries were digitised using the automated 'calcGrains' procedure through the MTEX toolbox with a 10° misorientation threshold to define single grains. Grain sizes of glaucophane, epidote and albite were determined by fitting ellipses to single grains and measured as the equivalent diameter derived from the grain area measured through an automated procedure in MTEX. Grain size results have been plotted in grain size histograms for each mineral analysed, along with mean and standard deviation. Similarly, in MTEX, fabric analysis was carried out by measuring the grain aspect ratios, calculated as the ratio between long and short axes of fitted ellipses, and the grain orientations, calculated as the angle of the fitted ellipse long axis to the stretching lineation (section 4.2). Grain aspect ratios were plotted against grain orientations to show the degree of shape-preferred orientation of each mineral phase.

4.2. Misorientation maps and LPO plots

Orientation data for glaucophane, epidote and albite were used to compile internal misorientation maps (mis2mean) and lattice preferred orientation (LPO) plots (section 4.3). The latter have been created based on the mean orientation of single grains. The mean orientation of each grain has been plotted on lower hemisphere, equal area projections. The M-index was calculated for each mineral, as a measure of LPO fabric strength from 0 for random fabrics to 1 for single crystal orientations (Skemer et al., 2005).

4.3. Amphibole chemistry

Amphibole compositions were measured through EDS. Compositional maps were acquired using a 20 kV voltage and the instrument was calibrated using kaersutite as standard to measure amphibole composition. Our measurements of the standard remained within a standard deviation of 0.5 wt% (typically <0.2 wt%) from the published values of the standard for all elements reported (details about the kaersutite composition and standard deviation of measurements are in Supplementary Table 3). Amphibole compositions were measured separately in cores and rims of grains from both the matrix and block. Mineral formula recalculation was carried out on the basis of 23 oxygens and 15 total cations. We plotted the recalculation made by the maximum of Fe^{3+}, obtained by following the Schumacher (1997) procedure for
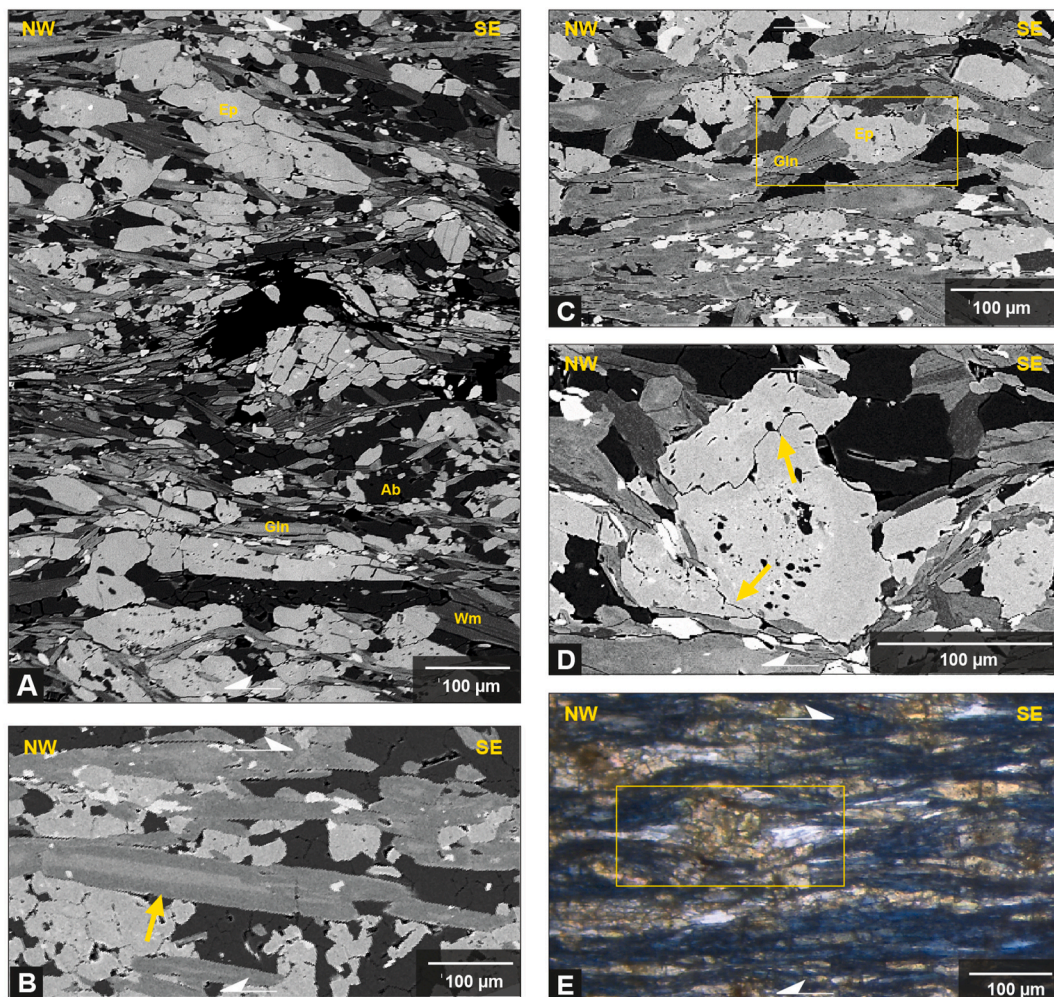

Fig. 3. a) Backscattered electron (BSE) image of the representative microstructure for the epidote-blueschist matrix. Glaucophane grains are aligned with the foliation surrounding grains of epidote and albite; b) BSE image with detail of glaucophane grains aligned with the foliation. The zoning pattern is parallel to the long axis of the crystal and it is not truncated; c) BSE image of the microfabric of the matrix. In the yellow box the development of glaucophane grains in the strain shadows of epidote grains is noticeable; d) BSE image of large epidote porphyroclasts. Yellow arrows indicate fractures; e) optical microscope photomicrograph (crossed-polarised light) of matrix fabric. In the yellow box the presence of albite grains in the strain shadows of epidote is noticeable. *Gln: glaucophane, Ep: epidote, Ab: albite.* (For interpretation of the references to colour in this figure legend, the reader is referred to the Web version of this article.)

calculation of minimum, average and maximum Fe^{3+} in amphiboles. Mineral analyses and recalculation for sodic amphiboles are reported in the Supplementary Data Tables 1 and 2

5. Microstructural analyses

5.1. Matrix and block microstructure

In this study, we focus on microstructures of the epidote-blueschist blocks and matrix rocks to consider the rheological differences causing the block-in-matrix structure to develop. Based on EBSD maps, the epidote-blueschist matrix contains a modal mineral assemblage of glaucophane (43%), epidote (27%), albite (18%), with minor white mica, quartz and titanite. The epidote-blueschist blocks have the same mineral assemblage as the matrix but lower glaucophane content, with epidote (45%), albite (24%), glaucophane (21%) and minor quartz and titanite. There are also greenschist blocks containing chlorite and Ca-rather than Na-amphibole in the area, but these are not considered further in this study on rheology of Na-amphibole rocks.

At the microscale, the matrix is characterized by continuous layers of glaucophane and minor white mica separating discontinuous domains of epidote, albite, quartz and minor titanite (Figs. 2B and 3A). Glaucophane long axes are generally parallel to the foliation, but locally are at a higher angle forming an oblique foliation consistent with a top to S/SE sense of shear. Glaucophane constitutes the main foliation and is also locally present in epidote strain shadows (Fig. 3C). Epidote, albite, quartz and titanite domains range in size from 100 μm to a few millimeters and have a lenticular shape that is only rarely asymmetric, in those cases consistent with a top to S/SE sense of shear. Epidote grains, in particular, are fractured and accompanied by strain shadows with fine-grained overgrowths of albite and, locally, glaucophane (Fig. 3D and E). Blocks have the same mineral assemblage as the matrix and are characterized by discontinuous domains of glaucophane and minor white mica alternating with mm-sized lenses of epidote, albite, quartz and titanite (Fig. 3D). The cores of the blocks are not as well-foliated as the matrix, with discontinuous layers of glaucophane separating grains of epidote and only locally domains of epidote and albite (Fig. 4A). Most of glaucophane grains occur with their long axes oblique to the foliation. Similar to the matrix, epidote grains are mostly fractured and present albite in their strain shadows (Fig. 4C).

The rims of the blocks show the same fabric characteristics as the matrix, with continuous layers of glaucophane separating grains of
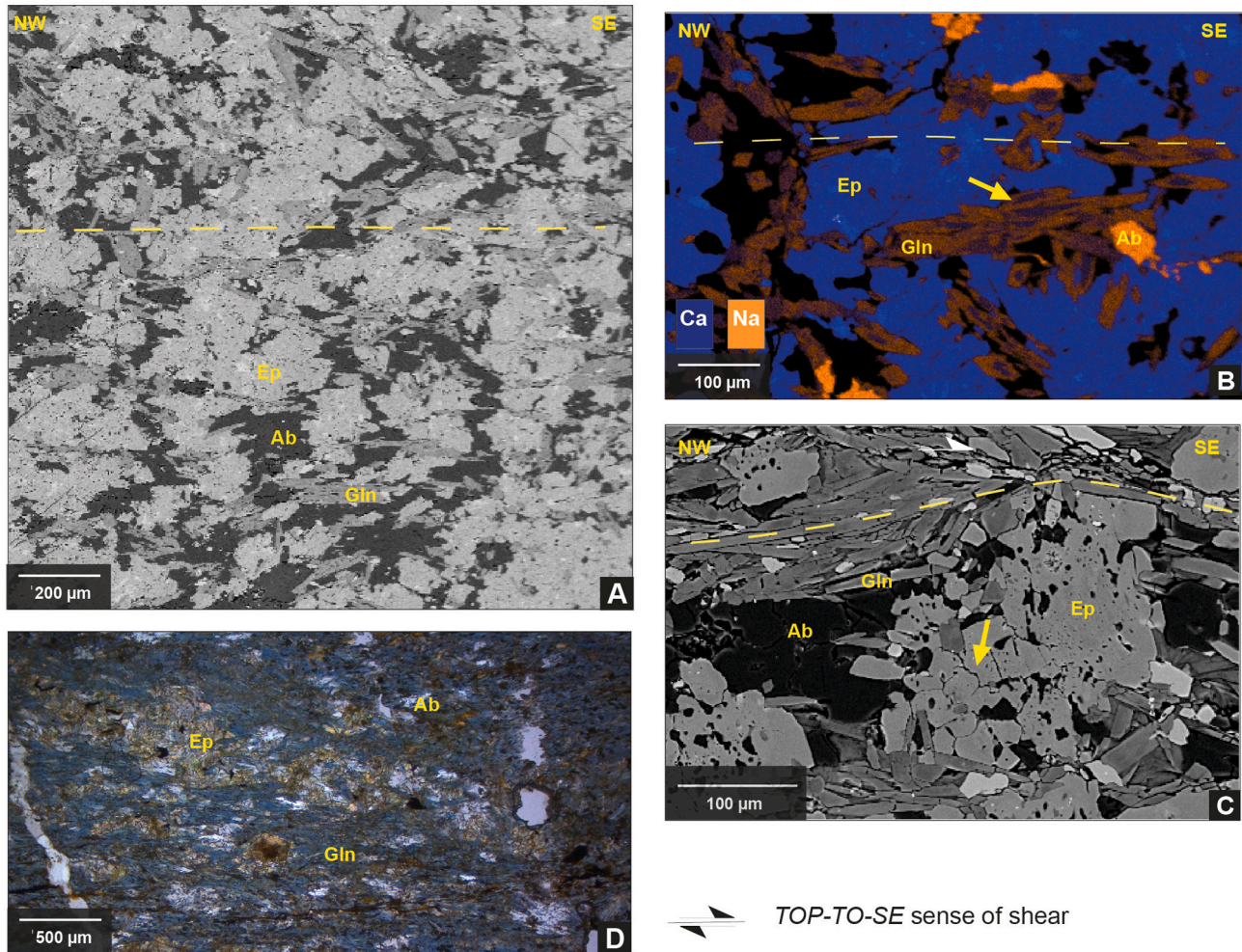

Fig. 4. a) Backscattered electron (BSE) image of the representative microstructure of the epidote-blueschist blocks. The glaucophane grains form discontinuous layers and are not well aligned with the foliation (yellow dashed line); b) EDS map of the epidote-blueschist block microfabric. Yellow arrow indicates the glaucophane grains. The map shows the zoning of the grains, mostly parallel to the crystals' long axis. The cores of the grains are richer in Ca, whereas the rims are richer in Na. blue: Ca, Orange: Na; c) BSE image of epidote grain. Yellow arrow indicates fractures within the grain. Note how albite grains develop in the epidote strain shadows; d) photomicrograph of the fabric that characterizes the rim of the epidote-blueschist block. Glaucophane grains form continuous layers, well aligned with the foliation. *Gln: glaucophane, Ep: epidote, Ab: albite*. (For interpretation of the references to colour in this figure legend, the reader is referred to the Web version of this article.)

epidote, albite and titanite (Fig. 4D).

Backscattered electron images show, in the matrix and blocks alike, that most glaucophane crystals are chemically zoned (Figs. 3B and 4B). Glaucophane cores are relatively rich in Ca and Mg and the rims are relatively rich in Na, with lower Ca and Mg content (Fig. 5A and B). EDS analyses (Table 1 in Supplementary Data) show that the cores have mostly a winchite composition, while the rims have a predominant glaucophane composition (Fig. 5C and D). The concentric zonation pattern is more developed along the grain long axis and less developed parallel to the short axis, showing that the chemical change is evident in both directions, normal to- and parallel to the grain elongation, with no evidence of truncated patterns. This concentric pattern is not systematic for all the grains, with a few of them presenting complex patterns that are not recognisable as core-to-rim variations nor as representing new grains. Epidote and albite grains do not appear to be zoned.

5.2. Grain size analysis

In the epidote-blueschist matrix, glaucophane grain sizes range from a few microns to 50 μm (mean 10 μm) and aspect ratios vary from 1 to 9 (Fig. 6A and B). Epidote grains are up to 100 μm (mean 11 μm) and aspect ratios vary from 1 to 5 (Fig. 6A and B). Albite size ranges from a few microns to 15 μm (mean 8 μm) with aspect ratios ranging from 1 to 5 (Fig. 6A and B). Although in general, glaucophane, epidote, and albite long axes orientations relative to the stretching lineation are scattered, the grains with the highest aspect ratios are aligned along the lineation suggesting that the matrix has a well-developed shape-preferred orientation (SPO) (Fig. 6B).

In the epidote-blueschist block, glaucophane grains have a broader grain size distribution compared to the matrix, ranging from a few microns up to 90 μm, but similar mean values (mean 13 μm), and aspect ratios of 1–7 (Fig. 6C and D). Epidote grains have a larger grain size than the matrix, with size up to 120 μm (mean 20 μm) and aspect ratios of 1–5 (Fig. 6C and D) and albite grains range in grain size from a few microns to 25 μm (mean 11 μm) and have aspect ratios ranging 1 to 3 (Fig. 6C and D). Here, there is a larger variation of orientation of glaucophane, epidote, and albite grains with respect to the lineation (Fig. 6D), and even the grains with the highest aspect ratios are not systematically aligned with the lineation, indicating that the epidote-blueschist blocks have a less developed SPO compared to the matrix.
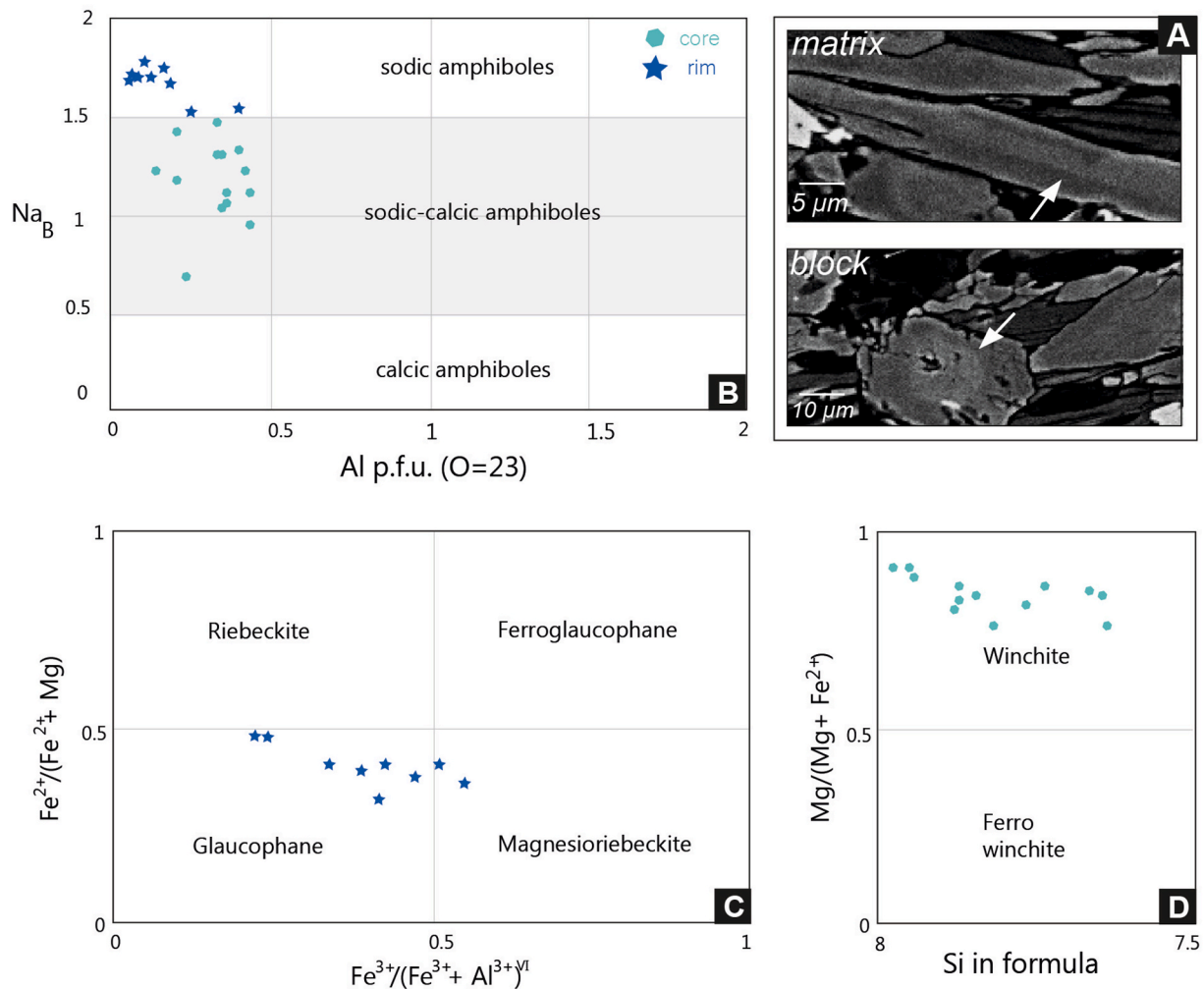

Fig. 5. EDS analyses of foliation-forming amphiboles in Tomuru metamorphic rocks. a) Backscatter images showing the detail of chemical zoning in the blue amphiboles in the matrix and in the block. Arrows indicate the concentric core-to-rim zonations present. The grain cores, lighter grey, are rich in Ca, while the rims, darker grey, are rich in Na; b) plot of the variation of Na content over Al content in the cores and rims of amphiboles. The cores contain X_{NaB} ranging 0.6–1.5, the rims contain X_{NaB} ranging 1.5–1.72; c) Composition diagram for the amphibole rims, falling in the magnesioriebeckite – glaucophane field; d) composition diagram of the amphibole cores, plotting in the winchite field. Compositional plots from Leake and Woolley, 1997). (For interpretation of the references to colour in this figure legend, the reader is referred to the Web version of this article.)
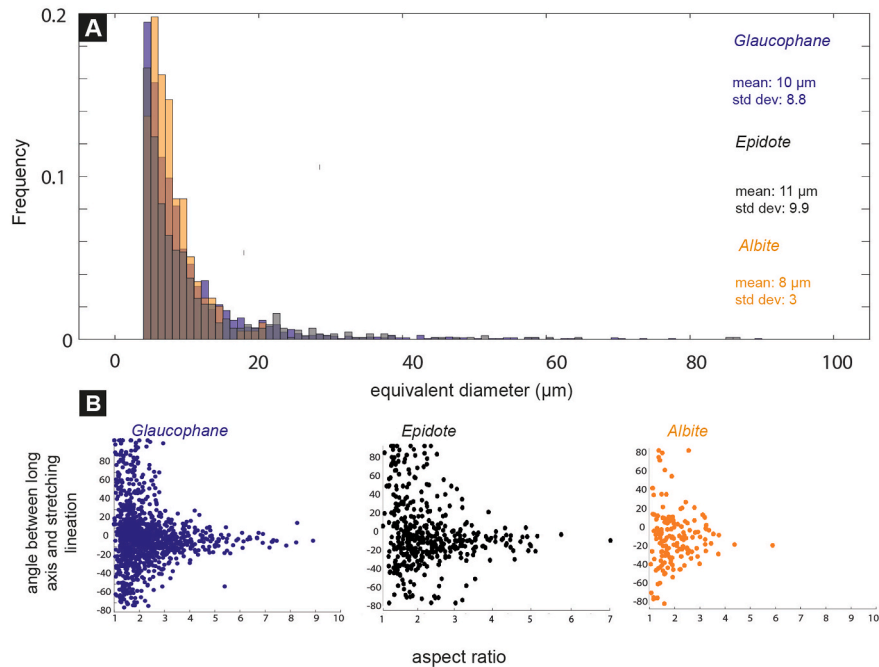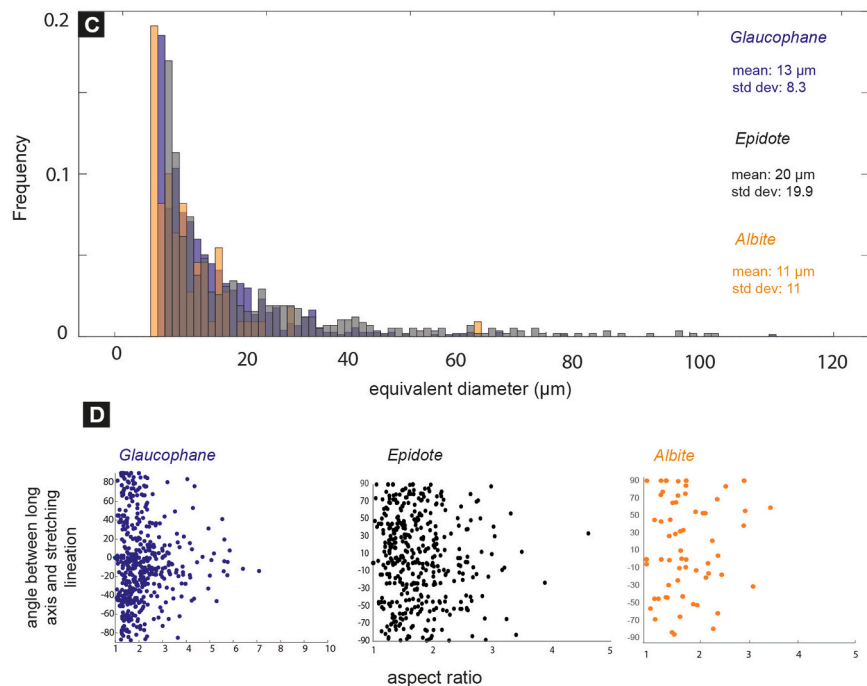
Fig. 6. Grain size and fabric analysis of the foliation-forming minerals in the matrix and the block. a) composite grain size histograms of glaucophane, epidote and albite in the matrix. Size mean and deviation standard are reported for each mineral; b) plots showing the relationship between grains aspect ratio versus angle to lineation for glaucophane, epidote and albite in the matrix. Orientations are scattered, however the grains with the highest aspect ratio are aligned along the lineation. Point per grain analysis; c) composite grain size histogram of glaucophane, epidote and albite in the block, with size mean and deviation standard reported for each mineral; d) plots showing the relationship between grain aspect ratio versus angle to lineation for glaucophane, epidote and albite in the block. The orientation are scattered and there is no pattern recognisable. Point per grain analysis.

5.3. EBSD analysis

Two matrix areas from the same thin section were analysed, as the microstructure of the matrix is heterogeneous, with glaucophane-rich (Fig. 7A,D,G) and epidote-rich portions (Fig. 7B,E,H). The glaucophane-rich portion is constituted for the most part by glaucophane (73% modal proportion; grain size up to 13 μm, mean 5 μm) with albite (8% modal proportion; grain size up to 23 μm) enveloping epidote domains (18%; 30–50 μm in size), whereas in the epidote-rich portion the glaucophane grains (32%; mean grain size 5 μm) are less interconnected and lie between numerous grains of epidote of much larger grain size (60%; 75–100 μm size range); here albite (7%) has size
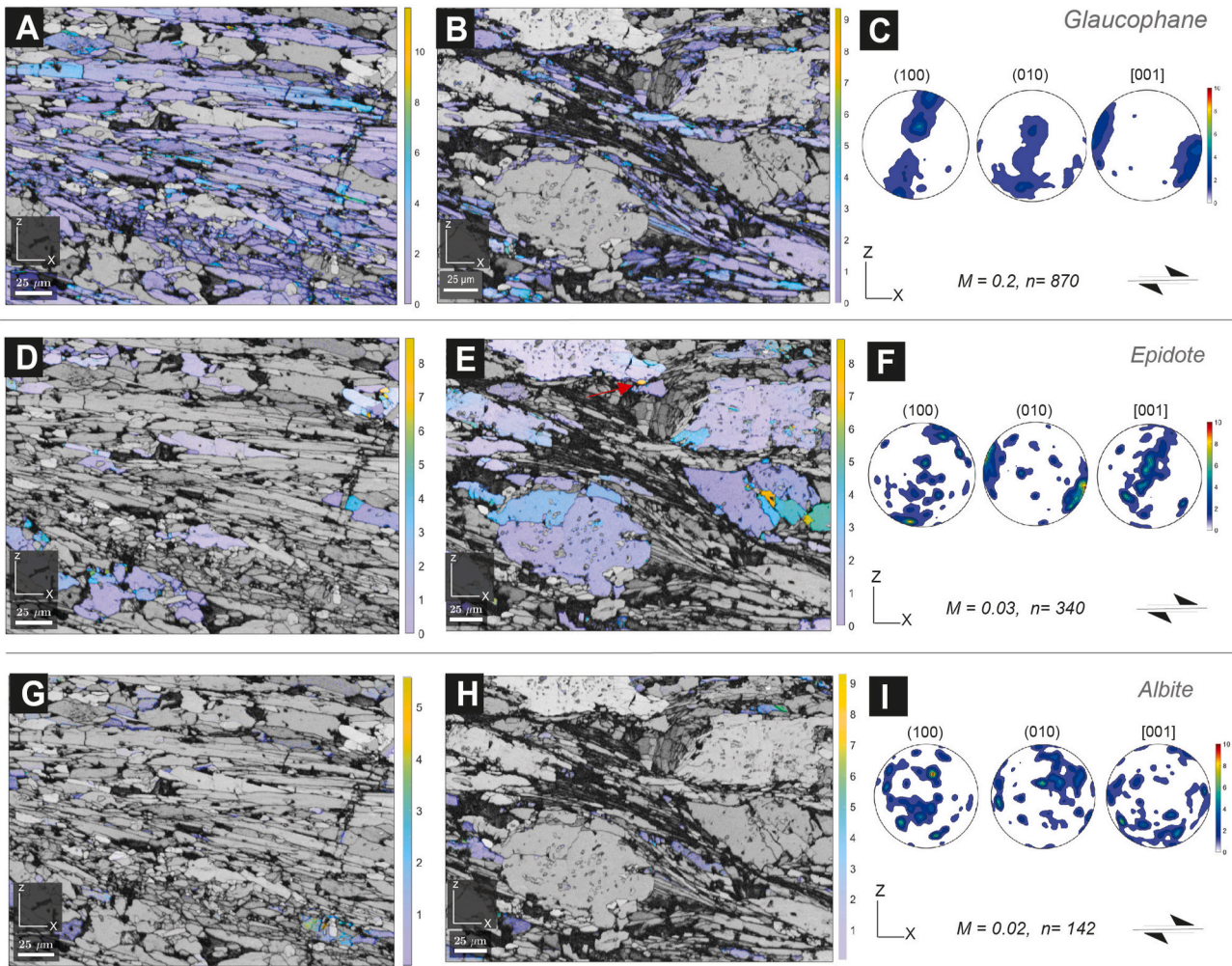
Fig. 7. EBSD analyses on foliation-forming minerals in the matrix. a) and b) glaucophane misorientation maps (mis2mean) in the glaucophane-rich (a) and epidote-rich area (b) respectively. Colour bars indicate the angles of misorientations. c) glaucophane LPO plots, point per grain analysis, lower hemisphere projections. D) and e) epidote misorientation maps (mis2mean) in the glaucophane-rich (d) and epidote-rich area (e) respectively, white arrows indicate possible subgrains. f) epidote LPO plots, point per grain analysis, lower hemisphere projections. g) and h) albite misorientation maps (mis2mean) in the glaucophane-rich (g) and epidote-rich area (h) respectively. i) Albite LPO plots, point per grain analysis, lower hemisphere projections. *M= Skemer index, n = number of grains*. (For interpretation of the references to colour in this figure legend, the reader is referred to the Web version of this article.)

up to 25 μm. In both matrix areas, EBSD analyses (Fig. 7A,B,C) show that foliation-forming glaucophane has very low misorientation angles (0–5°). The low degree and pattern of misorientations is not consistent with the formation of subgrains and does not suggest any significant crystal plasticity, with the highest misorientation angles corresponding to fractures within the grains (Fig. 7A and B). Moreover, the pattern of misorientation does not seem to be coincident with the chemical zoning of the glaucophanes. The glaucophane grains show a well-developed LPO, with poles to (100) sub-normal to foliation and [001] axes sub-aligned with the lineation both in the epidote-rich and glaucophane-rich portions (Fig. 7C). The glaucophane fabric strength has an M-index of 0.2.

EBSD analysis on epidote (Fig. 7D,E,F) shows different microstructures than glaucophane, both in magnitude and geometry of internal misorientation. Misorientation angles are greater (0–9°) and their pattern suggests misorientations along fractures in the larger grains with few local subgrains (Fig. 7D and E). LPO is not particularly strong (M = 0.03), with poles to (100) having a scattered distribution, poles to (010) sub-parallel to foliation (Fig. 7F) and [001] axes sub-normal to lineation. Finally, albite grains show very low degrees of internal misorientations (0–4°) (Fig. 7G and H), and very weak LPO (M = 0.02), with no recognisable pattern (Fig. 7I).

The fabric in the epidote-blueschist block sample is not as heterogeneous as in the matrix (Fig. 8). Throughout the thin section, glaucophane grains are poorly connected and separate domains of coarser-grained epidote, albite and titanite. Therefore, only one area, representative of the fabric, has been analysed. Here, similar to what was measured in the matrix, glaucophane shows low misorientation angles (0–7°), and the pattern of misorientations is not consistent with formation of subgrains (Fig. 8A), not coincident with the chemical zonations within the grains, and not aligned along fractures. LPO patterns show a more dispersed girdle than in the matrix, poles to (100) are sub-normal to the foliation and [001] axes are sub-parallel to the lineation with a more diffuse distribution. Here, the LPO is more scattered than in the matrix, with M-index = 0.07, substantially lower than the M-index for the epidote-blueschist matrix (Fig. 8A).

In the block, epidote grains show a higher degree of internal misorientation than the glaucophane, with angles locally up to 12° (Fig. 8B) and the pattern resembles subgrains only where misorientation angles are larger. There is no lattice-preferred orientation, with no alignment in the principal directions. The fabric strength is slightly lower than in the matrix (M = 0.02). Albite microstructures show a low degree of internal misorientation and weak LPO (M = 0.02) with poles to (100) showing a highly dispersed girdle and [001] axes highly scattered
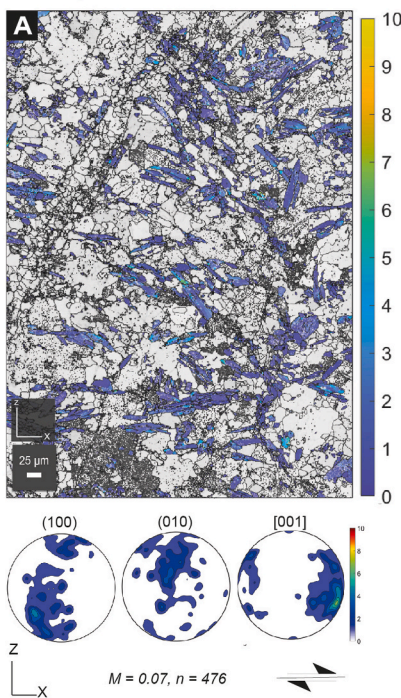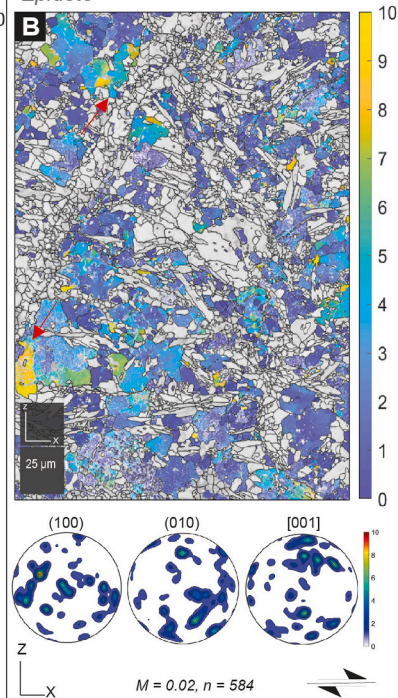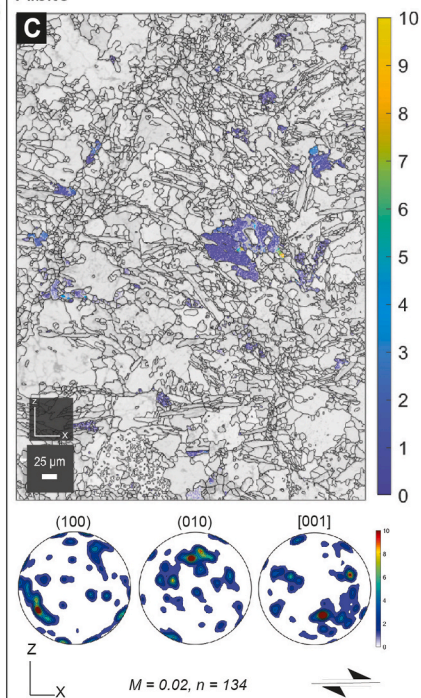
Fig. 8. EBSD analysis on foliation-forming minerals in the block. a) misorientation map (mis2mean) for glaucophane and glaucophane LPO plots, point per grain analysis, lower hemisphere projections. b) Epidote misorientation map (mis2mean) and LPO plots, point per grain analysis, lower hemisphere projections. c) Albite misorientation map (mis2mean) and LPO plots, point per grain analysis, lower area projection. *M= Skemer index, n = number of grains.*

(Fig. 8C).

In the analysed samples, the M-index of fabrics in the epidote-blueschist matrix is low overall (0.2–0.02), but significantly higher than the M-index (0.07–0.02) of fabrics in the epidote-blueschist block. This comparison shows that the matrix has a better developed fabric than the blocks, consistent with mesoscale observations**.**

6. Discussion

6.1. Deformation mechanisms in the Tomuru epidote-blueschists

Our microstructural observations on samples of the Tomuru metamorphic rocks show that the epidote-blueschist matrix is characterised by two portions that differ in relative abundance of minerals and grain size of epidote (Fig. 7). The portion with high relative abundance of glaucophane and where epidote grain size is smaller represents a high strain domain of well-developed foliation and LPO (Fig. 7A,D,G). In contrast, the portion where epidote is more abundant and grain size is larger represents a relatively low strain domain of poorly developed foliation and poor LPO (Fig. 7B,E,H). In the relatively high strain domain, very low degrees of intracrystalline misorientations within the glaucophane grains, along with the absence of clear evidence of dislocation creep microstructures (e.g., undulose extinction, subgrains) exclude significant deformation by movement of dislocations. Moreover, the small grain size of glaucophane (mean: 10 μm) fits well with the grain size that is observed to effectively promote diffusive mechanisms in minerals in shear zones (Tsenn and Carter, 1987; Tullis and Yund, 1991; Stenvall et al., 2019). Concentric core-to-rim compositional variations in glaucophane grains, more developed along the long axes of the grains, parallel to the stretching lineation (Figs. 3B and 4B), are interpreted as the result of compositional changes acquired during subduction-related metamorphism, with increasing Na as pressure increases, as has been described in other high-pressure terranes

(Nakamura and Enami, 1994). The geometry of zonation reinforces the interpretation that fabric-forming glaucophane grains deformed by diffusive mass transfer (e.g., Giuntoli et al., 2018) and were not the product of passive rotation and subsequent oriented growth. The presence of glaucophane grains in epidote strain shadow, although local, may suggest that there is contribution of pressure solution, although the absence of truncation of chemical patterns, as well as the absence of solution seams in these samples, suggests that contribution of pressure solution to deformation might not be significant, favouring the interpretation of predominant deformation by diffusion and reaction creep. The syn-deformation chemical changes within the amphibole grains, along with the well-developed shape preferred orientation, suggest that metamorphic reactions operating during diffusion-controlled deformation in glaucophane might have contributed to glaucophane fabric formation, by changing amphibole composition during progressive deformation, as pressure increased, and by aligning the glaucophane grains along foliation, in orientations favourable for them to effectively deform by diffusive mechanisms. Microstructural analysis on glaucophane fabric shows that a well-defined SPO developed during deformation by diffusion creep and reaction mechanisms can coexist with the development of a well-defined LPO, which is therefore not necessarily the product of dislocation creep in glaucophane.

Epidote microstructures show some differences from glaucophane: grains have a larger grain size, SPO is not well developed, and while the degree of internal misorientation is generally low, locally, epidote crystals have misorientation patterns suggesting development of subgrains (Fig.. 7E and 8B). Although the LPO is less developed than in glaucophane, it is defined by a relatively dispersed girdle. These observations suggest that epidote grains might have experienced some very incipient, low strains by dislocation creep in the high strain domain. That said, the epidote grains are largely undeformed, and have behaved relatively rigidly with some fractures, so such local dislocation creep in epidote is not an important mechanism for bulk deformation of these

rocks.

The albite crystals have small grain size, poorly developed SPO and LPO, and suggest deformation by diffusive mechanisms. The overgrowth in pressure shadows on epidote suggests that pressure solution was active during deformation of albite, although the absence of chemical zonation, as well as evidence for truncation around albite grains, does not allow us to infer with certainty the importance of this component of diffusion. It is difficult to infer the degree to which reaction-driven creep contributed to form albite fabric, as there is no significant chemical zoning or strain localization in the grains.

In the low strain domain, glaucophane and albite microstructures are comparable to those observed in the high strain domain, whereas epidote has higher degrees of internal misorientation, and, only locally, misorientations resemble subgrains, tentatively suggesting that dislocation creep played a minor role. However, LPO is very poorly developed, and the highest internal misorientations are limited to grains in epidote-rich domains (Fig. 7E and F) or to fractures within coarser epidote grains. These characteristics are likely indicative of dominantly passive grain rotation, with some intragrain deformation through fracturing, alongside incipient dislocation creep to small finite strains.

In summary, glaucophane grains have characteristics typical of diffusion creep, likely accompanied by reaction-driven creep, and similarly, albite deformed by a diffusive mechanism. In contrast, epidote deformation is characterised by passive grain rotation with intragrain fracturing and incipient dislocation creep. The geometry of the fabric, in which glaucophane forms interconnected layers that surround the epidote and albite grains, leads us to conclude that the predominant deformation mechanism controlling matrix rheology is diffusion and reaction creep in glaucophane. That a combination of diffusion and reaction can control amphibole deformation is not a new conclusion (e.g. Berger and Stünitz, 1996; Imon et al., 2004; Giuntoli et al., 2018; Soret et al., 2019; Lee et al., 2022; Muñoz-Montecinos et al., 2023), but a key point here is that such diffusion-reaction creep dominates at epidote-blueschist conditions in a block-in-matrix subduction interface shear zone, where blocks and matrix are defined by different viscosities during diffusive deformation.
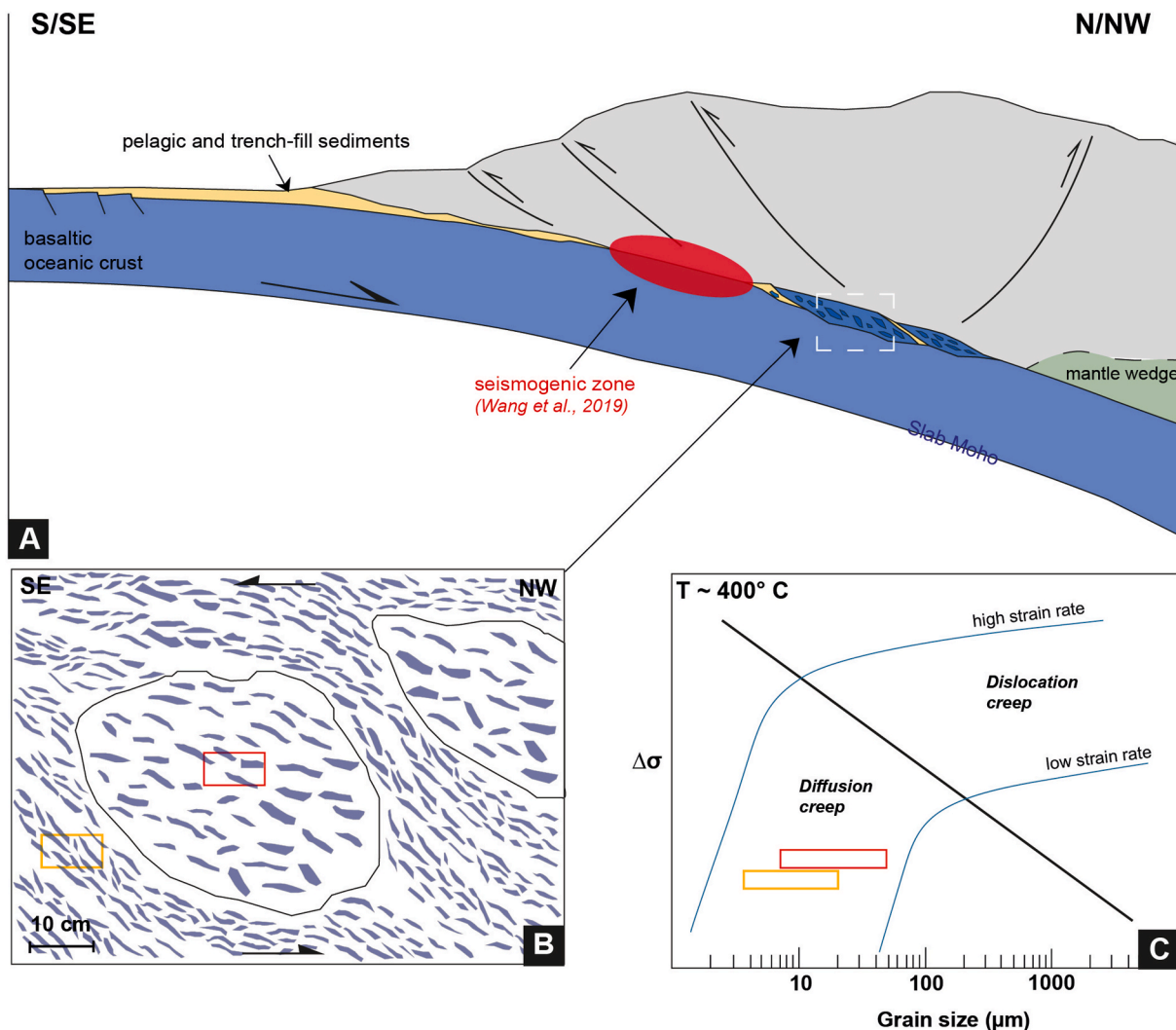

Fig. 9. a) Qualitative cross section sketch of a convergent margin showing the approximate setting of exhumed Tomuru epidote-blueschists. In red, the location of the seismogenic zone interpreted by Wang et al. (2019). b) Schematic cartoon representative of the different foliation development of the block-in-matrix Tomuru blueschists. In blue, foliation drawn as glaucophane grains (not in scale). In yellow and red, the representation of matrix and block samples analysed. c) Qualitative sketch of an approximate deformation mechanism map for glaucophane, with the diffusion creep field being predominant at lower stress conditions. We chose to represent only dislocation creep as representative at higher stresses in our samples. Dislocation glide and/or cataclastic deformation may be possible at higher stresses, but that have not been shown because they are so far unknown in detail. Red box represents epidote-blueschist block, yellow box represents the matrix. The length of the boxes refers to the range in glaucophane grain size, the vertical position has been chosen arbitrarily within the field of diffusion creep, representing the interpreted higher stress in the block and lower stress in the matrix. (For interpretation of the references to colour in this figure legend, the reader is referred to the Web version of this article.)

The heterogeneity within the matrix, with differences in fabric and strain of the glaucophane-rich and epidote-rich end-member domains at a millimeter scale, is equivalent to the difference between epidote-blueschist blocks and the matrix at multi-dm scale. In this sense, the blocks are similar to the low strain domains in the matrix, as their microstructures are comparable.

The difference between high and low strain portions of matrix and blocks at the mesoscale is potentially guided by glaucophane microfabrics. The presence of interconnected networks of glaucophane separating isolated domains of epidote and albite implies that strain is localised in the epidote-blueschist matrix, relative to the blocks. Moreover, diffusion creep accompanied by reaction creep as the predominant deformation mechanisms is indicative of a low stress domain. In the block, glaucophane does not form well-interconnected layers, and is located between more abundant and larger grains of epidote. Because epidote can be considered more competent than glaucophane, based on its relatively rigid and undeformed appearance, the block may have experienced higher stress despite the lower strain.

To better visualise these interpretations, a qualitative deformation mechanism map for glaucophane in our samples is shown in Fig. 9. The plot illustrates the difference in fabric development between the blocks and the matrix: the matrix shows a well-defined foliation with glaucophane having well-developed SPO and LPO patterns, whereas the blocks retain a less pervasive foliation, with glaucophane having less well-defined SPO and LPO patterns (Fig. 9B). These small differences in fabric imply a relatively small competency contrast between the blocks and the matrix, thus lacking substantial viscosity gradients. However, the variation in grain size and fabric development also implies higher stress in the lower strain blocks, which is compatible with expectations from numerical models of higher strain rate flow around more rigid blocks (Beall et al., 2019; Behr et al., 2021) – although again the viscosity contrast must have been relatively low for the blocks not to deform more (Beall et al., 2019). The difference in stress conditions must also be small enough to favour deformation by diffusion creep, accompanied by reaction-driven creep, in both block and matrix, as observed from the microstructures. Moreover, it can be argued that the small competency contrast inferred between block and matrix, along with the microstructural evidence, implies that the shear stress is too low to initiate deformation by dislocation creep, except in a few higher stress locations, favouring diffusive mechanisms instead.

6.2. Implications for stress on the plate interface and seismic style

Although there are no previous studies with detailed interpretation of the tectonic origin of Tomuru epidote-blueschists, the block-in-matrix structure with consistent asymmetry that characterizes the Tomuru metamorphic rocks represents shear zone structure typical of the melanges commonly characterising the subduction interface (Shreve and Cloos, 1986; Fagereng and Sibson, 2010; Kimura et al., 2012; Rowe et al., 2013) (Fig. 7A). Moreover, in the preserved epidote-blueschist mineral assemblage, zonation indicative of progressive growth during subduction allows us to interpret that the Tomuru epidote-blueschists were subject of high pressure and relative low temperature metamorphism during deformation, which is typical of subduction zones (Miyashiro, 1961; Ernst, 1973; Maekawa et al., 1993). Moreover, the epidote-blueschist blocks and matrix have the same mineralogy, and the change of fabric from the core to the rim of the blocks, suggests that the block-in-matrix fabric of the Tomuru metamorphic rocks forms as the consequence of different strain localization processes, from block to matrix, during subduction-related deformation. This strain localization is, at least in the final product, a function of slightly finer grain size and a more interconnected glaucophane fabric, and thus more efficient diffusion and reaction creep. Several processes may have initiated these differences, including different grain size and/or fabric in the protolith, cataclastic grain size reduction, or metamorphic or metasomatic grain size and fabric evolution. We do not have the data to separate these

options, but emphasize the importance of grain size and fabric, whatever their origin, as controls on strain localization in these epidote-blueschist rocks.

In terms of plate interface rheology, low stress conditions and high fluid pressure have been related to slow earthquakes (Kodaira et al., 2004; Audet et al., 2009; Fagereng et al., 2011; Ujiie et al., 2018). These conditions are also important if we consider the role fluids and stress levels have on which type of diffusion mechanism can be active on the plate interface. In the presence of a fluid phase, generally at low temperature and slow shear strain rates, dissolution-precipitation creep is considered to be dominant (Wassmann and Stöckhert, 2013; Tulley et al., 2020; Malvoisin and Baumgartner, 2021), as opposed to solid-state diffusion, which happens at higher temperatures than dissolution-precipitation creep, and where diffusion occurs either along grain boundaries (Coble creep) or through the crystal lattice (Nabarro-Herring creep) (Rutter, 1976; Wheeler, 1992). In the Tomuru metamorphic rocks we might currently not be able to discern whether solid-state diffusion or fluid-assisted diffusion is predominant. Tomuru metabasites have fewer veins than exhumed subduction complexes such as the Coastal Makimine Mélange and Nagasaki Metamorphic Rocks in Kyushu, where fluid-related deformation is thought to be enhanced by local or nearby dehydration reactions (Tulley et al., 2022; Ujiie et al., 2022), or blueschist in the Zagros suture zone that preserve vein networks indicative of episodic fluid injection and brittle deformation (Muñoz-Montecinos et al., 2023). The presence of veins in this study suggests that fluids were present; however, more data to constrain the timing and deformation conditions of the veins compared to the metabasites, are needed to clarify the amount to which veining contributed to deformation of the mafic rocks at epidote-blueschist facies conditions. Based on the data available, some fluid may have aided diffusion along grain boundaries and leading to overgrowths in pressure shadows, but likely not enough to create a pervasive dissolution-precipitation related foliation.

We can conclude with more certainty that local stress during deformation of the Tomuru epidote-blueschists must have been low enough to maintain diffusion and/or reaction creep as the predominant mineral-scale deformation mechanism in the interconnected glaucophane ± albite that controlled bulk-rock rheology. In order to change the predominant deformation mechanism from diffusion to dislocation creep, at fixed strain rate, pressure and temperature, stress should be locally and transiently elevated, especially when grain size is very small (Fig. 9C). To further quantify stresses, rheological relations need to be carefully defined by relating microstructures and fabric analysis with geologically realistic strain rates.

Examples of studies on rheology of natural blueschists are rare in literature, and the Tomuru epidote-blueschists differ when compared to some other natural examples. Some studies observe close association of blueschist rocks to eclogite, where the heterogeneity induced by the dehydration of glaucophane-rich blueschist to form higher viscosity eclogite causes local stress increases that could possibly promote dislocation creep in glaucophane (Behr et al., 2018). Other studies investigating fabrics of natural lawsonite blueschists interpret the formation of glaucophane during exhumation, as suggested by the change in chemical composition within the grains, with decrease of Na from core to rim (Kim et al., 2013). The authors suggest deformation by dislocation creep during exhumation and retrogressive metamorphism. Yet other studies point out the role of diffusive deformation mechanisms in amphibole-rich rocks, similarly to what we describe for the Tomuru metamorphic rocks; however, these authors highlight fracturing and fluid flow at grain boundaries to facilitate dissolution-precipitation creep as the bulk deformation mechanism for amphibole (Giuntoli et al., 2018; Muñoz-Montecinos et al., 2023), which partially differs from our observations where there is little evidence for fracturing/cataclasis accompanying the diffusion and reaction creep in glaucophane.

In terms of plate interface seismic style, the generally low inferred

shear stress and the small inferred stress gradients between blocks and matrix could facilitate steady creep in the deep subduction interface, because transients are unlikely to develop if stresses and deformation mechanisms are both relatively constant in time and space. This inference is consistent with general low stress conditions, and although it is important to consider that deformation is potentially sensitive to local changes in strain rate or fluid pressure. Episodic tremor and slow slip require episodic transient stress changes to occur. To create conditions where the plate interface could move transiently rather than by steady creep, it would be necessary to impose a stress or strain rate change (e.g., Beall et al., 2019), for example through a nearby earthquake, larger competency contrast between blocks and matrix, or by transient weakening though fluid pressure pulses driven by dehydration reactions during prograde deformation. Such changes may occur if epidote-blueschist rocks are subducted deeper and epidote and glaucophane dehydrate, at temperatures exceeding 500 °C or more (dependent also on pressure, Fagereng and Diener, 2011). This can lead to a fluid pressure increase at the sort of depths at which slow slip occurs in the relatively cold Alaska subduction margin (e.g. Ohta et al., 2006; Li et al., 2016).

7. Conclusions

We quantified fabric development of an epidote-blueschist block-in-matrix association, showing that despite the same mineralogy, blocks and matrix preserve differences in fabric development. The blocks have poorly developed foliation and LPO compared to the matrix in which they are embedded. From microstructural analyses of the main foliation-forming minerals glaucophane, albite and epidote, both matrix and block rheology are controlled by diffusion and reaction creep of fabric-forming glaucophane, diffusion creep in albite, and with minor incipient dislocation creep and fracturing in relatively rigid epidote. The inferred fabric development and deformation microstructures suggest that during deformation on the plate interface, local stress levels were low to explain lack of significant deformation in the dislocation creep regime in any of the minerals.

As literature on natural blueschist deformation mechanisms is limited, our observations underline the importance of diffusive and reaction-driven creep processes governing fabric development of subducting epidote-blueschists, and at a bigger scale, plate interface rheology in the depth range for ETS below the thermally-controlled seismogenic zone. Our observations imply that at epidote-blueschist conditions, glaucophane-controlled deformation by distributed diffusion creep can occur at low stress, and influx of fluids or a transient stress increase is needed to change the rheology and generate instabilities. Further quantification of stresses, indispensable for accurate modelling of stability fields of deformation mechanisms, requires an amphibole flow law and its extrapolation to geological strain rates.

CRediT authorship contribution statement

Sara De Caroli: Conceptualization, Methodology, Investigation, Writing – original draft, Writing – review & editing, Visualization. **Åke Fagereng:** Conceptualization, Writing – review & editing, Supervision, Project administration. **Kohtaro Ujiie:** Supervision, Writing – review & editing. **Thomas Blenkinsop:** Conceptualization, Supervision, Writing – review & editing. **Francesca Meneghini:** Supervision, Writing – review & editing. **Duncan Muir:** Resources, Writing – review & editing.

Declaration of competing interest

The authors declare that they have no known competing financial interests or personal relationships that could have appeared to influence the work reported in this paper.

Appendix A. Supplementary data

Supplementary data to this article can be found online at https://doi.org/10.1016/j.jsg.2023.105041.

References

Audet, P., Bostock, M.G., Christensen, N.I., Peacock, S.M., 2009. Seismic evidence for overpressured subducted oceanic crust and megathrust fault sealing. Nature 457, 76–78.

Bachmann, F., Hielscher, R., Schaeben, H., 2010. Texture analysis with MTE-free and open source software toolbox. Solid State Phenom. 160, 63–68.

Beall, A., Fagereng, Å., Ellis, S., 2019. Strength of strained two-phase mixtures: application to rapid creep and stress amplification in subduction zone mélange. Geophys. Res. Lett. 46 (1), 169–178.

Behr, W.M., Bürgmann, R., 2021. What's down there? The structures, materials and environment of deep-seated slow slip and tremor. Philosophical Transactions of the Royal Society A 379, 20200218.

Behr, W.M., Gerya, T.V., Cannizzaro, C., Blass, R., 2021. Transient slow slip characteristics of frictional-viscous subduction megathrust shear zones. AGU Advances 2 (3), e2021AV000416.

Behr, W.M., Kotowski, A.J., Ashley, K.T., 2018. Dehydration-induced rheological heterogeneity and the deep tremor source in warm subduction zones. Geology 46, 475–478.

Berger, A., Stünitz, H., 1996. Deformation mechanisms and reaction of hornblende: examples from the Bergell tonalite (Central Alps). Tectonophysics 257 (2–4), 149–174.

Brodie, K.H., Rutter, E.H., 1985. On the relationship between deformation and metamorphism, with special reference to the behaviour of basic rocks. In: Advances in Physical Geochemistry, ume 4. Springer.

Condit, C.B., Mahan, K.H., 2018. Fracturing, fluid flow and shear zone development: relationships between chemical and mechanical processes in Proterozoic mafic dykes from southwestern Montana, USA. J. Metamorph. Geol. 36 (2), 195–223.

Ernst, W.G., 1973. Blueschist metamorphism and PT regimes in active subduction zones. Tectonophysics 17 (3), 255–272.

Fagereng, Å., Sibson, R.H., 2010. Mélange rheology and seismic style. Geology 38, 751–754.

Fagereng, Å., Diener, J.F., 2011. Non-volcanic tremor and discontinuous slab dehydration. Geophys. Res. Lett. 38, L15302.

Fagereng, Å., Remitti, F., Sibson, R.H., 2011. Incrementally developed slickenfibers—geological record of repeating low stress-drop seismic events? Tectonophysics 510, 381–386.

Fagereng, Å., Hillary, G.W., Diener, J.F., 2014. Brittle-viscous deformation, slow slip, and tremor. Geophys. Res. Lett. 41, 4159–4167.

Fisher, D., Byrne, T., 1987. Structural evolution of underthrusted sediments, Kodiak Islands, Alaska. Tectonics 6 (6), 775–793.

Getsinger, A.J., Hirth, G., 2014. Amphibole fabric formation during diffusion creep and the rheology of shear zones. Geology 42 (6), 535–538.

Giuntoli, F., Menegon, L., Warren, C.J., 2018. Replacement reaction and deformation by dissolution and precipitation processes in amphibolites. J. Metamorph. Geol. 36, 1263–1286.

Heki, K., Kataoka, T., 2008. On the biannually repeating slow-slip events at the Ryukyu Trench, southwestern Japan. J. Geophys. Res. 113, B11402.

Hyndman, R.D., Yamano, M., Oleskevich, D.A., 1997. The seismogenic zone of subduction thrust faults. Isl. Arc 6, 244–260.

Imon, R., Okudaira, T., Kanagawa, K., 2004. Development of shape- and lattice-preferred orientations of amphibole grains during initial cataclastic deformation and subsequent deformation by dissolution-precipitation creep in amphibolites from the Ryoke metamorphic belt, SW Japan. J. Struct. Geol. 26, 793–805.

Ishizuka, H., Imaizumi, M., 1988. Metamorphic aragonite from the Yaeyama metamorphic rocks on Ishigaki- jima, Southwest Ryukyu islands. J. Geol. Soc. Jpn. 94 (9), 719–722.

Kim, D., Katayama, I., Michibayashi, K., Tsujimori, T., 2013. Rheological contrast between glaucophane and lawsonite in naturally deformed blueschist from Diablo Range, California. Isl. Arc 22, 63–73.

Kimura, G., Yamaguchi, A., Hojo, M., Kitamura, Y., Kameda, J., Ujiie, K., Hamada, Y., Hamahashi, M., Hina, S., 2012. Tectonic melange as fault rock of subduction plate boundary. Tectonophysics 568 – 569, 25–38.

Kirkpatrick, J.D., Fagereng, Å., Shelly, D.R., 2021. Geological constraints on the mechanisms of slow earthquakes. Nat. Rev. Earth Environ. 2, 285–301.

Kizaki, K., 1986. Geology and tectonics of the Ryukyu islands. Tectonophysics 125, 193207.

Kilian, R., Heilbronner, R., Stünitz, H., 2011. Quartz grain size reduction in a granitoid rock and the transition from dislocation to diffusion creep. J. Struct. Geol. 33 (8), 1265–1284.

Kodaira, S., Kato, A., Park, O.J., Iwasaki, T., Yoshiyuki, T., et al., 2004. High fluid pressure may cause silent slip in the Nankai Trough. Science 304, 1295–1298.

Kotowski, A., Behr, W.M., 2019. Length scales and types of heterogeneities along the deep subduction interface: insights from exhumed rocks on Syros Island, Greece. Geosphere 15.

Lallemand, S., Liu, C., Dominguez, S., Schnurle, P., Malavielle, J., ACT Scientific Crew, 1999. Trench-parallel stretching and folding of forearc basins and lateral migration of the accretionary wedge in the southern Ryukyus: a case of strain partition caused by oblique convergence. Tectonics 18 (2), 231–247.

Leake, B.E., Woolley, A.R., 1997. Nomenclature of amphiboles: report of the subcommittee on amphiboles of the international mineralogical association, commission on new minerals and mineral names. Can. Mineral. 35, 219–246.

Lee, A., Stünitz, H., Soret, M., Ariel Battisti, M., 2022. Dissolution precipitation creep as a process for the strain localisation of amfic rocks. J. Struct. Geol. 155, 104505.

Li, S., Freymueller, J., McCaffrey, R., 2016. Slow slip events and time-dependent variations in locking beneath Lower Cook Inlet of the Alaska-Aleutian subduction zone. J. Geophys. Res. Solid Earth 121 (2), 1060–1079.

Maekawa, H., Shozui, M., Ishli, T., Fryer, P., Pearce, J., 1993. Blueschist metamorphism in an active subduction zone. Nature 364.

Malvoisin, B., Baumgartner, L.P., 2021. Mineral dissolution and precipitation under stress: model formulation and application to metamorphic reactions. G-cubed 22 (5).

Misch, P., 1969. Paracrystalline microboudinage of zoned grains and other criteria for synkinematic growth of metamorphic minerals. Am. J. Sci. 267, 43–63.

Miyashiro, A., 1961. Evolution of metamorphic belts. J. Petrol. 2 (3), 277–311.

Montési, L.G., Hirth, G., 2003. Grain size evolution and the rheology of ductile shear zones: from laboratory experiments to postseismic creep. Earth Planet Sci. Lett. 211 (1–2), 97–110.

Muñoz-Montecinos, J., Angiboust, S., Garcia-Casco, A., Raimondo, T., 2023. Shattered veins elucidate brittle creep processes in the deep Slow Slip and Tremor region. Tectonics 42, e2022TC007605.

Nakamura, C., Enami, M., 1994. Prograde amphiboles in hematite-bearing basic and quartz schists in the Sanbagawa belt, field gradient and P-T paths of individual rocks. J. Metamorph. Geol. 12, 841–852.

Nakamura, M., 2017. Distribution of low-frequency earthquakes accompanying the very low frequency earthquakes along the Ryukyu Trench. Earth Planets Space 69, 49. https://doi.org/10.1186/s40623-017-0632-4.

Nyman, M.N., Law, R.D., Smelik, A., 1992. Cataclastic deformation mechanism for the development of core-mantle structures in amphiboles. Geology 20, 455–458.

Nuong, N.D., Itaya, T., Nishimura, Y., 2008. Age (K-Ar phengite)-temperature-structure relations: a case study from the Ishigaki high-pressure schist belt, southern Ryukyu Arc, Japan. Geol. Mag. 145 (5), 677–684.

Obara, K., 2002. Nonvolcanic deep tremor associated with subduction in Southwest Japan. Science 296, 1679–1681.

Obara, K., Hirose, H., Yamamizu, F., Kasahara, K., 2004. Episodic slow slip events accompanied by non-volcanic tremors in southwest Japan subduction zone. Geophys. Res. Lett. 31, L23602.

Obara, K., Kato, A., 2016. Connecting slow earthquakes to huge earthquakes. Science 353 (6296), 253–257.

Ohta, Y., Freymueller, J.T., Hreinsdóttir, S., Suito, H., 2006. A large slow slip event and the depth of the seismogenic zone in the south central Alaska subduction zone. Earth Planet Sci. Lett. 247 (1–2), 108–116.

Oncken, O., Angiboust, S., Dresen, G., 2022. Slow slip in subduction zones: reconciling deformation fabrics with instrumental observations and laboratory results. Geosphere 18 (1), 104–129.

Osozawa, S., Wakabayashi, J., 2012. Exhumation of Triassic HP-LT rocks by upright extrusional domes and overlying detachment faults, Ishigaki-jima, Ryukyu islands. J. Asian Earth Sci. 59, 70–84.

Peacock, S.M., 1992. Blueschist-facies metamorphism, shear heating, and P-T-t paths in subduction zones. J. Geophys. Res. 97, 17693–17707.

Peng, Z., Gomberg, J., 2010. An integrated perspective of the continuum between earthquakes and slow-slip phenomena. Nat. Geosci. 3, 599–607.

Reynard, B., Gillet, P., 1989. Deformation mechanisms in naturally deformed glaucophanes – a Tem and Hrem study. Eur. J. Mineral 1, 611–624.

Rogers, G., Dragert, H., 2003. Episodic tremor and slip on the Cascadia subduction zone: the chatter of silent slip. Science 300, 1942–1943.

Rowe, C., Moore, J.C., Remitti, F., 2013. The thickness of subduction plate boundary faults from the seafloor into the seismogenic zone. Geology 41 (9), 991–994.

Rutter, E.H., 1976. The kinetics of rock deformation by pressure solution. Transactions of the Royal Society of London 283, 203–219.

Rutter, E., Brodie, K., 1988. The role of tectonic grain size reduction in the rheological stratification of the lithosphere. Geol. Rundsch. 77 (1), 295–307.

Schmalzle, G., McCaffrey, R., Creager, K.C., 2014. Central Cascadia subduction zone creep. G-cubed 15, 1515–1532.

Schumacher, J.C., 1997. The estimation of ferric iron in electron microprobe analysis of amphiboles. Am. Mineral. 82, 643–651.

Schwartz, S.Y., Rokosky, J.M., 2007. Slow slip events and seismic tremor at circum-pacific subduction zones. Rev. Geophys. 45.

Skemer, P., Katayama, I., Jiang, Z., Karato, S., 2005. The misorientation index: development of a new method for calculating the strength of lattice-preferred orientation. Tectonophysics 411 (1), 157–167.

Shea, W.T., Kroonenberg, A.K., 1993. Strength and anisotropy of foliated rocks with vaaries mica contents. Journal fo Structural Geology 15 (9–10), 1092–1121.

Shreve, R.L., Cloos, M., 1986. Dynamics of sediment subduction, melange formation, and prism accretion. J. Geophys. Res. 91 (B10), 10229–10245.

Stenvall, C., Fagereng, A., Diener, J.F.A., 2019. Weaker than weakest: on the strength of shear zones. Geophys. Res. Lett. 46, 7404–7413.

Skrotzki, W., 1990. Microstructure in Hornblende of a Mylonitic Amphibolite, vol. 54. Geological Society, London, Special Publications, pp. 321–325.

Suenaga, N., Yoshioka, S., Ji, Y., 2021. 3-D thermal regime and dehydration processes around the regions of slow earthquakes along the Ryukyu Trench. Sci. Rep. 11, 11251 https://doi.org/10.1038/s41598-021-90199-2.

Tsenn, M.C., Carter, N.L., 1987. Upper limits of power law creep of rocks. Tectonophysics 13 (1–2), 1–26.

Tulley, C., Fagereng, A., Ujiie, K., 2020. Hydrous oceanic crust hosts megathrust creep at low shear zones. Sci. Adv. 6, eaba1529.

Tulley, C.J., Fagereng, Å., Ujiie, K., Diener, J.F.A., Harris, C., 2022. Embrittlement within viscous shear zones across the base of the subduction thrust seismogenic zone. G-cubed 23, e2022GC010569.

Tullis, J., Yund, R.A., 1991. Diffusion creep in feldspar aggregates: experimental evidence. J. Struct. Geol. 13 (9), 987–1000.

Ujiie, K., Saishu, H., Fagereng, Å., Nishiyama, N., Otsubo, M., Masuyama, H., Kagi, H., 2018. An explanation for episodic tremor and slow slip constrained by crack-seal veins and viscous shear in subduction mélange. Geophys. Res. Lett. 45, 5371–5379.

Ujiie, K., Noro, K., Shigematsu, N., Fagereng, Å., Nishiyama, N., Tulley, C.J., Masuyama, H., Mori, Y., Kagi, H., 2022. Megathrust shear modulated by albite metasomatism in subduction mélanges. G-cubed 23, e2022GC010569.

Wang, S., Hsu, S., Yeh, Y., 2019. Earthquake-related structures beneath the southernmost portion of the Ryukyu Arc and forearc. Geophys. Res. Lett. 46, 3717–3725.

Wassmann, S., Stöckhert, B., 2013. Rheology of the plate interface – dissolution precipitation creep in high pressure metamorphic rocks. Tectonophysics 608, 1–29.

Wheeler, J., 1992. Importance of pressure solution and Coble creep in the deformation of polymineralic rocks. J. Geophys. Res. 97, 4579–4586.

Weertman, J., 1968. Dislocation climb theory of steady-state creep. Transactions of the American Society of Metals 61, 681.

Wintsch, R.P., Christoffersen, R., Kroenenberg, A.K., 1995. Fluid-rock reaction weakening of fault zones. J. Geophys. Res. 100, 13021–13032.

Wintsch, R.P., Yi, K., 2002. Dissolution and replacement creep: a significant deformation mechanism in mid-crustal rocks. J. Struct. Geol. 24, 1179–1193.

Wintsch, R.P., Yeh, M., 2013. Oscillating brittle and viscous behavior through the earthquake cycle in the Red River Shear Zone: monitoring flips between reaction and textural softening and hardening. Tectonophysics 587, 46–62.